

## Synthesis and Raman spectroscopy of a layered SiS<sub>2</sub> phase at high pressures

Yu Wang, Shu-Qing Jiang, Alexander F. Goncharov, Federico A. Gorelli, Xiao-Jia Chen, Dušan Plašienka, Roman Martoňák, Erio Tosatti, and Mario Santoro

Citation: *The Journal of Chemical Physics* **148**, 014503 (2018);

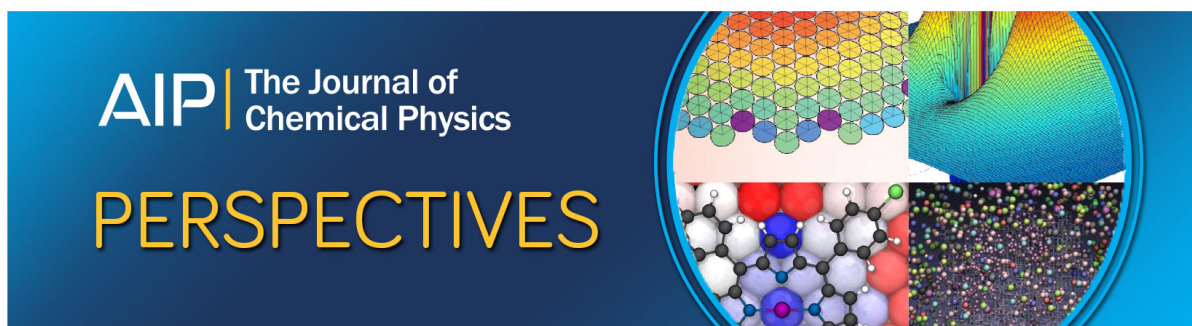
View online: <https://doi.org/10.1063/1.5011333>

View Table of Contents: <http://aip.scitation.org/toc/jcp/148/1>

Published by the [American Institute of Physics](#)

---

---



# Synthesis and Raman spectroscopy of a layered SiS<sub>2</sub> phase at high pressures

 HPSTAR  
 523-2018

 Yu Wang,<sup>1,2</sup> Shu-Qing Jiang,<sup>1</sup> Alexander F. Goncharov,<sup>1,3</sup> Federico A. Gorelli,<sup>4</sup> Xiao-Jia Chen,<sup>5</sup> Dušan Plašienka,<sup>6</sup> Roman Martoňák,<sup>6</sup> Erio Tosatti,<sup>7,8</sup> and Mario Santoro<sup>4,a)</sup>
<sup>1</sup>Key Laboratory of Materials Physics and Center for Energy Matter in Extreme Environments, Institute of Solid State Physics, Chinese Academy of Sciences, 350 Shushanghu Road, Hefei, Anhui 230031, China

<sup>2</sup>University of Science and Technology of China, Hefei 230026, Anhui, People's Republic of China

<sup>3</sup>Geophysical Laboratory, Carnegie Institution of Washington, 5251 Broad Branch Road, Washington, DC 20015, USA

<sup>4</sup>Istituto Nazionale di Ottica (CNR-INO) and European Laboratory for non Linear Spectroscopy (LENS), Via N. Carrara 1, 50019 Sesto Fiorentino, Italy

<sup>5</sup>Center for High Pressure Science and Technology Advanced Research, Shanghai 201203, China

<sup>6</sup>Department of Experimental Physics, Faculty of Mathematics, Physics and Informatics, Comenius University in Bratislava, Mlynská dolina F2, 84248 Bratislava, Slovakia

<sup>7</sup>International School for Advanced Studies (SISSA) and CNR-IOM Democritos, Via Bonomea 265, 34136 Trieste, Italy

<sup>8</sup>The Abdus Salam International Centre for Theoretical Physics (ICTP), Strada Costiera 11, 34151 Trieste, Italy

(Received 31 October 2017; accepted 18 December 2017; published online 3 January 2018)

Dichalcogenides are known to exhibit layered solid phases, at ambient and high pressures, where 2D layers of chemically bonded formula units are held together by van der Waals forces. These materials are of great interest for solid-state sciences and technology, along with other 2D systems such as graphene and phosphorene. SiS<sub>2</sub> is an archetypal model system of the most fundamental interest within this ensemble. Recently, high pressure (GPa) phases with Si in octahedral coordination by S have been theoretically predicted and also experimentally found to occur in this compound. At variance with stishovite in SiO<sub>2</sub>, which is a 3D network of SiO<sub>6</sub> octahedra, the phases with octahedral coordination in SiS<sub>2</sub> are 2D layered. Very importantly, this type of semiconducting material was theoretically predicted to exhibit continuous bandgap closing with pressure to a poor metallic state at tens of GPa. We synthesized layered SiS<sub>2</sub> with octahedral coordination in a diamond anvil cell at 7.5-9 GPa, by laser heating together elemental S and Si at 1300-1700 K. Indeed, Raman spectroscopy up to 64.4 GPa is compatible with continuous bandgap closing in this material with the onset of either weak metallicity or of a narrow bandgap semiconductor state with a large density of defect-induced, intra-gap energy levels, at about 57 GPa. Importantly, our investigation adds up to the fundamental knowledge of layered dichalcogenides. *Published by AIP Publishing.* <https://doi.org/10.1063/1.5011333>

## I. INTRODUCTION

The class of 2D materials is commonly thought to constitute one of the leading candidates toward new technologies, which could influence practically all fields of human activity in the near future.<sup>1</sup> Beyond graphene, current research is now focusing on other bi-dimensional compounds such as phosphorene and dichalcogenides. 2D materials are made of either a single layer or a few layers of a 3D parent bulk layered solid, such as graphite for graphene, where layers of chemically bonded formula units are held together by van der Waals forces and can be easily exfoliated. Dichalcogenides are a broad class of materials exhibiting layered phases, whose structural and transport properties can be well tuned by applied pressure. For instance, in transition metal dichalcogenides, several high pressure, solid-solid phase transitions have been found so far

between layered phases, usually connected to the insulator-to-semimetal transition driven by the optical bandgap closing.<sup>2-6</sup> Other possibilities include structural transitions which still preserve the 2D layered character, e.g., a layer sliding transition found in MoS<sub>2</sub><sup>2,4,7,8</sup> or an increase of coordination inside the layers predicted in MoTe<sub>2</sub>.<sup>9</sup> At even higher pressures in the Mbar range, the layered character may be lost and genuine 3D phases are formed instead as predicted, e.g., in MoS<sub>2</sub> and MoSe<sub>2</sub>.<sup>9,10</sup>

SiS<sub>2</sub> belongs to this important class of compounds and, specifically, to the subclass of group IV dichalcogenides such as CO<sub>2</sub>, SiO<sub>2</sub>, GeO<sub>2</sub>, and CS<sub>2</sub>. The sequence of phases of silicon-disulfide observed in the range 0-6 GPa includes four different structures, all made of SiS<sub>4</sub> tetrahedra with increasing connectivity from 1D to 3D upon increasing pressure and with van der Waals interaction between chains (1D connectivity) and between layers (2D connectivity).<sup>11-19</sup> Very recently, evolutionary search based on density functional theory (DFT) calculations surprisingly predicted three different 2D layered

<sup>a)</sup>Email: santoro@lens.unifi.it

phases in  $\text{SiS}_2$ :  $P\bar{3}m1$ ,  $P6_3mc$ , and  $R\bar{3}m$ , with silicon in octahedral coordination by sulfur, to become more stable than the tetrahedrally coordinated phases above 4 GPa,  $P\bar{3}m1$  being the most stable structure up to 100 GPa.<sup>20</sup> In all these phases, the  $\text{SiS}_6$  units share their edges within the layers, which in turn interact only via van der Waals forces. The tetrahedral-octahedral switch is quite general in group IV compounds upon compression, but there are also remarkable differences among these systems. For instance, in  $\text{SiO}_2$  and  $\text{CO}_2$ , the coordination increase of Si and C leads to full 3D networks rather than layers above 10 GPa and 800 GPa, respectively.<sup>21,22</sup> Interestingly, all the three layered octahedral phases of  $\text{SiS}_2$  were theoretically found to undergo a continuous pressure-induced decrease of the indirect bandgap until metallization<sup>20</sup> with no further structural changes, a behavior that  $\text{SiS}_2$  shares with other dichalcogenides<sup>4-7,23</sup> and that, for this particular system, was predicted to lead to metallization at around 30 GPa, within the Generalized Gradient Approximation (GGA) for the exchange-correlation functional. On the other hand, since the GGA approximation tends to underestimate the value of the bandgap and, consequently, the pressure of metallization, the electronic band structure calculations were repeated for the  $P\bar{3}m1$  structure also using the HSE06 hybrid functional that includes exact exchange, which is thereby a more reliable approximation in this respect.<sup>20</sup> In this case, the bandgap was found to be equal to about 2 eV at 10 GPa and metallization was predicted to occur at 40 GPa. At this pressure, the gap closes by band overlap between the  $\Gamma$  point (top of the valence band, with large S-character) and the K-point (bottom of the conduction band, with large Si-character), and above this pressure,  $\text{SiS}_2$  remains a rather poor metal with low density of states (DOS) near the Fermi energy even at 100 GPa. Indeed, DOS at the Fermi energy is lower than its maximum value by one order of magnitude, still at 100 GPa. The theoretical robustness of the  $P\bar{3}m1$  layered phase then also suggested possible recovery at ambient pressure, even in a single monolayer, which in turn would be a real 2D system. In a parallel experimental investigation, the  $P\bar{3}m1$  phase was indeed obtained upon compression of  $\text{SiS}_2$  above 7.4 GPa, as shown by structural refinement of the X-ray diffraction patterns, which were measured up to 30 GPa.<sup>24</sup> Also, Raman spectra reported up to 44 GPa at just four selected pressures exhibit only two vibrational peaks in the 270-540  $\text{cm}^{-1}$  frequency range, consistent with Raman active vibrational modes predicted by group theory for the  $P\bar{3}m1$  space group. On the other hand, that study does not provide quantitative clues on pressure behavior of the bandgap although it is reported that the sample was changing the color from white at low pressure to yellow and brown to black at the maximum pressure. Here we present a study on  $\text{SiS}_2$  under pressure in a diamond anvil cell (DAC), where layered, octahedrally coordinated  $\text{SiS}_2$  was first directly synthesized by laser heating a mixture of the elements Si and S at 7.5-9 GPa and then compressed up to about 64 GPa. Accurate determination of pressure dependence of intensity and line-shape for the Raman peaks indicates a continuous bandgap closing finally leading, at about 57 GPa, to either metallization or a narrow bandgap semiconductor state with a large density of defect-induced, intra-gap energy levels. Overall, our experimental results are compatible with DFT predictions on

pressure-induced bandgap closing of these materials although onset pressure values differ slightly.

## II. METHODS AND PROCEDURES

$\text{SiS}_2$  is extremely hygroscopic and all contact with air moisture must be avoided during DAC loading procedures. At variance with previous experimental work under pressure, where  $\text{SiS}_2$  was synthesized from the vapor of the elements in a silicon glass tube and then transferred in the DAC with no pressure transmitting medium (PTM),<sup>24</sup> we synthesized the compound *in situ* from the elements directly in the DAC with argon as the PTM. Our DAC was equipped with 300  $\mu\text{m}$  culet beveled diamonds and a Re gasket with an initial hole of typically 100  $\mu\text{m}$  diameter and 40  $\mu\text{m}$  thickness. We then inserted two chips of powder clusters of high purity elemental S and Si, respectively, one on top of the other in the sample chamber together with a ruby chip for pressure measurements based on the ruby fluorescence method<sup>25</sup> (Fig. 1), and argon was finally gas-loaded at 2000 bars. The S and Si chips were of typical lateral size of 20-30  $\mu\text{m}$ , Si being slightly smaller than S. After loading, the Si/S sample was compressed at room temperature and the Raman spectrum was measured with pressure steps of about 1 GPa, up to about 7.5 GPa. At the highest pressure, the spectra showed a sharp phonon peak of crystalline Si and a broad doublet for S-S stretching in S, which was amorphous as a result of combined compression and green laser irradiation (Refs. 26 and 27 and references therein) (Fig. 1). We then laser-heated the Si/S sample at the starting pressure of 7.5 GPa up to 1300-1700 K, over an area of less than  $15 \times 15 \mu\text{m}^2$ , in order to melt together and react elemental Si and S. The choice of this pressure for laser heating was accurately made for at least two reasons. First, the melting temperature of Si is close to its minimum value, near to 1000 K at 10 GPa,<sup>28</sup> while the melting temperature of S is below 1000 K.<sup>29</sup> Second, the octahedral  $\text{SiS}_2$  material we wish to study becomes stable precisely at and above this pressure.<sup>20,24</sup> After laser heating, the sample was temperature-quenched with a final

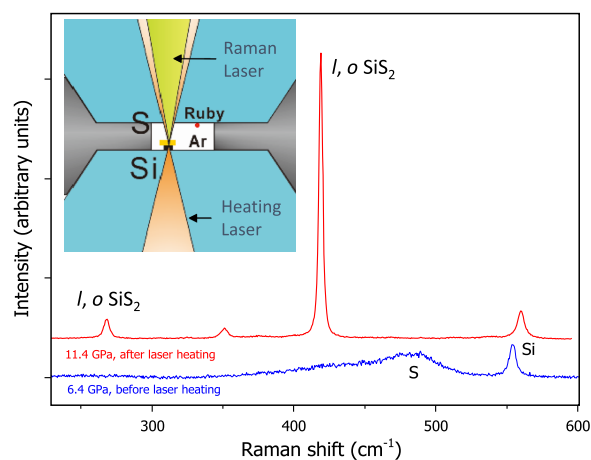


FIG. 1. Raman spectra of the Si/S mixture under pressure, before (elemental Si and S) and after (layered, *l*, octahedral, *o*  $\text{SiS}_2$ ) laser heating. Inset: sample configuration. Blue and grey: diamond anvils and gasket. Yellow and black slabs: S and Si, respectively. Horizontal arrows at the top and at the bottom point to green and near IR laser beams used for Raman spectroscopy and for sample heating (double side), respectively.

pressure of about 9 GPa where layered, octahedral  $\text{SiS}_2$  was detected over a reduced area with a lateral size of a few microns, as indicated by the two sharp Raman peaks at around  $270\text{ cm}^{-1}$  and  $420\text{ cm}^{-1}$ , respectively, already assigned to this material<sup>24</sup> (Fig. 1). The additional weak peak at around  $350\text{ cm}^{-1}$ , which rapidly disappears upon increasing pressure (Fig. 2), is likely to be due to a metastable remnant of the low-pressure tetrahedral phase.<sup>24</sup> This high pressure-high temperature synthesis procedure of  $\text{SiS}_2$  has been found to be very reproducible.

Double-sided laser heating was performed by using a CW solid-state laser at 1064 nm with a maximum power of 40 W. The laser was split into two beams, which were then focused on the two opposite sample sides through two 10 $\times$  near-infrared (NIR) Mitutoyo micro-objectives, respectively, down to spots with a lateral size of a few microns. Temperature measurements based on thermal radiation spectroscopy were conducted at both heated sides. Based on preliminary separate laser heating tests on pure Si and S, we realized that Si efficiently absorbed the NIR laser at our pressures, whereas the absorption by S was rather poor. Therefore, in the case of the Si/S mixture, it was mainly Si that was heated up by the laser, subsequently transferring the heat to the attached

S chip. We performed laser heating through a mesh of about  $15 \times 15\ \mu\text{m}^2$ , step  $5\ \mu\text{m}$ , with a heating time of about 10 s per point. Raman spectroscopy was then carried out on the temperature-quenched sample by using the 532 nm line of a frequency doubled Nd:YAG laser as the excitation source. Backscattering geometry was used with a 20 $\times$  micro-objective, with a few microns laser spot. The signal, once filtered by notch filters, was detected by a single Acton/SpectraPro 2500i monochromator, equipped with a CCD detector (Princeton Instruments, PIXIS: 400). The Raman spectral resolution was about  $1\text{ cm}^{-1}$ , and Raman diamond edge was also used to measure pressures.<sup>30</sup> In this study, a selected sample of layered octahedral  $\text{SiS}_2$  was compressed up to about 64 GPa and Raman spectra were measured upon increasing pressure.

Theoretical Raman spectra of layered, octahedral  $\text{SiS}_2$  were calculated within the local-density approximation (LDA) by the Quantum Espresso package,<sup>31</sup> which calculates besides phonon frequencies the non-resonant Raman intensities using the second-order response.<sup>32</sup> Norm-conserving Perdew-Zunger (LDA) pseudopotentials were employed along the energy cutoff of 950 eV for plane wave expansion. Fine k-point meshes of  $35 \times 35 \times 21$  were used for 3-atomic  $P\bar{3}m1$  unit-cells at all pressures.

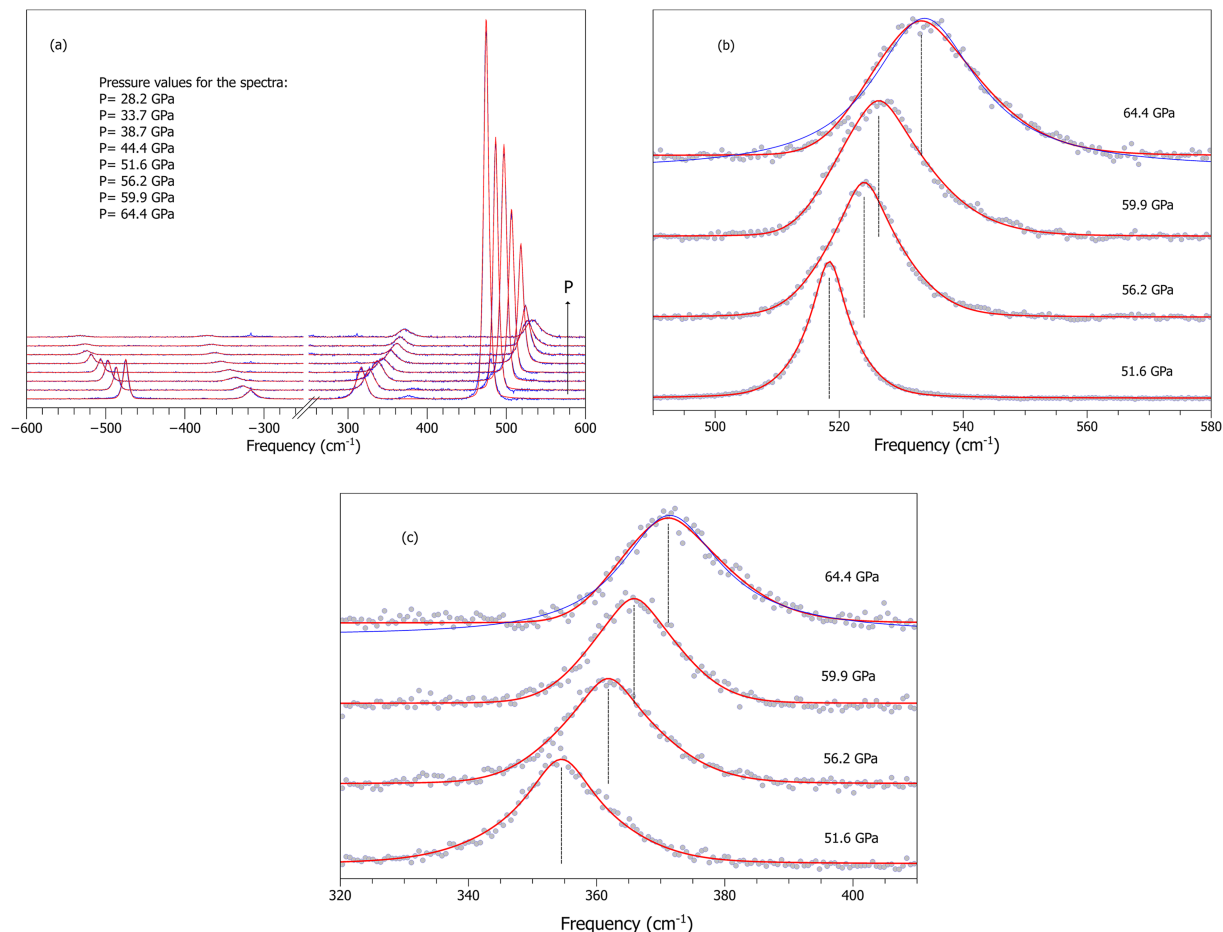


FIG. 2. (a) Selection of Stokes and anti-Stokes Raman spectra of temperature-quenched, layered, octahedral  $\text{SiS}_2$  measured upon increasing pressure up to 64.4 GPa (blue lines), together with the fitting function of Eq. (1) for all peaks (red lines). Spectral intensities have been normalized by the integrated intensity of the Stokes diamond peak. [(b) and (c)] Sub-selection of spectra for the two Stokes Raman peaks, respectively, showing the pressure-induced broadening and asymmetry (see text). Dots: experimental spectra; red lines: fitting function of Eq. (1); blue, continuous line at 64.4 GPa: Fano line-shape fit. Spectral intensities have been normalized by the same peak intensity and then vertically shifted for the sake of clarity.

### III. RESULTS AND DISCUSSIONS

In Fig. 2, we report a selection of Raman spectra of temperature-quenched, layered, octahedral SiS<sub>2</sub> measured upon compression up to about 64.4 GPa, together with a fitting function, which we will further discuss below. The weak and broad peaks of residual amorphous S along with a linear background have been subtracted out in the fitting procedure. Note the positive pressure shift and the pressure-induced line broadening for both sharp peaks, along with a general intensity decrease upon increasing pressure by about one (slightly less than one) order of magnitude for the high frequency (low frequency) peak [Fig. 2, panel (a)]. We can reasonably attribute the intensity drop to two simultaneous and independent effects, both related to either pressure-induced approaching of metallization or transformation to a narrow bandgap semiconductor with a large number of defect-related, intra-gap energy levels. One effect is the increase of optical absorption and the consequent decrease of the scattering volume, which can amount to an optical wavelength or less in the metallic or nearly metallic state, and the other effect is the Raman cross section reduction. This reduction, in turn, originates from the dielectric function becoming very large and complex and, as a consequence, rather insensitive to phonon driven fluctuations. Therefore, the Raman intensity drop is well compatible with this material undergoing pressure-induced bandgap closing, as predicted by DFT simulations;<sup>20</sup> on the other hand, this phenomenon is likely to occur within the same phase since we do not observe changes in the number of Raman peaks. It should be noted however that the intensity drop alone is caused by optical absorption at 532 nm and does not therefore support the transformation to a metallic state or to a strongly defective narrow bandgap semiconductor sufficiently. A much more stringent proof of this type of transformations is our additional observation of pressure-induced line-shape asymmetry. Beginning at some pressure, i.e., at about 57 GPa, both Raman peaks suddenly develop an increasing asymmetry, with a more marked broadening on the high frequency side [Fig. 2, panels (b) and (c)]. Several potential reasons for this pressure-induced asymmetry such as occurrence of a phase transition and sample bridging between the diamonds can be straightforwardly ruled out. At a phase transition, new Raman peaks should appear or, at least, the phase transition should affect the smoothness of the pressure shift of Raman frequencies, which was not the case here (see Fig. 3). Then, the thickness of the SiS<sub>2</sub> sample was always smaller than the gasket thickness along the entire compression run, as we checked by using white light fringes of transmitted light along with direct observations through the microscope, which totally ruled out the possibility of sample bridging. Therefore, it is very reasonable to suggest a different origin for the peak asymmetry. Indeed, we suggest that this asymmetry can only arise if the sample is metallic or nearly metallic because only this type of states possesses very low frequency electron-hole pair excitations with which the optical phonon modes can resonate and interfere. As described long ago by Fano (see Ref. 33 and references therein), the increasing line-shape asymmetry provides a measure of the rate of interference, which in the present case is proportional, through Fermi's golden rule, to the metallic or nearly metallic density

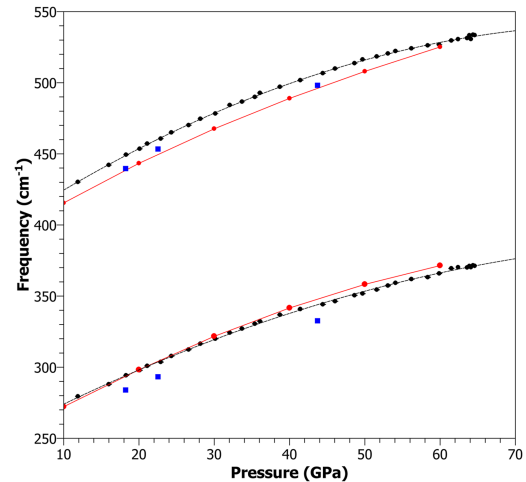


FIG. 3. Pressure shift of the two mode frequencies of layered, octahedral SiS<sub>2</sub> observed in this work (black circles), together with literature experimental data (blue squares)<sup>24</sup> and calculated in this work DFT values for the *P3m1* phase (red circles). Second-order polynomial curves,  $p + qP + rP^2$ , have been fit to the experimental data points of this work (black lines), with  $p = 247.1 \text{ cm}^{-1}$  ( $391.2 \text{ cm}^{-1}$ ),  $q = 2.829 \text{ GPa}^{-1} \text{ cm}^{-1}$  ( $3.542 \text{ GPa}^{-1} \text{ cm}^{-1}$ ), and  $r = -1.406 \times 10^{-2} \text{ GPa}^{-2} \text{ cm}^{-1}$  ( $-2.093 \times 10^{-2} \text{ GPa}^{-2} \text{ cm}^{-1}$ ). The values in parenthesis are for the high frequency mode.

of states close to the Fermi level. As a proof of metallization, Fano's line-shape asymmetry was used, for example, for heavily doped crystalline silicon,<sup>33</sup> germanium, and GaAs.<sup>34</sup> In undoped crystalline silicon, germanium, and GaAs, the Raman peak for the optical phonon has a Lorentzian line-shape, appropriate for a damped harmonic oscillator. In heavily doped samples, instead, the line-shape turns to an asymmetrically distorted Lorentzian,<sup>33,34</sup> similar to ours, which increases upon increasing the level of doping, i.e., of metallicity. We first tried to fit the very same model line-shape to the peaks of our SiS<sub>2</sub> material to establish the onset of transition to the metallic or highly defective narrow bandgap semiconductor state and then derive the pressure dependence of metallicity. Nevertheless, the quality of the fit was not entirely satisfactory [see the blue, continuous lines in Fig. 2, panels (b) and (c) for the maximum pressure] since our line-shapes exhibit some amount of Gaussian, i.e., inhomogeneous character. For this reason, following the main idea of an asymmetric line-shape due to free electrons, we empirically fit to our peaks an asymmetric pseudo-Voigt function<sup>35</sup>

$$I(\nu) = A \left\{ (1 - m) \sqrt{\frac{4 \ln(2)}{\pi \sigma^2(x)}} \exp \left[ - \left( \frac{4 \ln(2)}{\sigma^2(x)} \right) x^2 \right] + \frac{m}{2\pi} \frac{\sigma(x)}{\left( \frac{\sigma(x)}{2} \right)^2 + 4x^2} \right\}, \quad (1)$$

where  $\sigma(x) = \frac{2\sigma_0}{1 + e^{-ax}}$  and  $x = \nu - \nu_0$ .

In this analytical expression,  $\nu$  is the Raman shift, the parameter  $m$  balances the homogeneous Lorentzian to the inhomogeneous Gaussian character of the line-shape, and  $a$  drives the asymmetry. Equation (1) was then fit to both the Stokes and anti-Stokes peaks. Stokes and anti-Stokes components in each Stokes/anti-Stokes pair were constrained to the same values of the fitting parameters  $\sigma_0$ ,  $a$ ,  $\nu_0$ , whereas

$m$  is the same for all peaks. The results were excellent, as shown in Fig. 2, allowing us to discuss the pressure behavior of frequency, intensity, and line-shape based on this procedure. It is worth stressing once again that the choice of Eq. (1) as the asymmetric fitting function to the Raman peaks has a pure empirical ground, although this choice was constrained by at least two important requirements: (i) the function should fit the peaks very well and (ii) it should mimic the asymmetry character of the true Fano's line-shape. It is not unlikely that other suitable asymmetric functions either based on physical models or just empirical could be found, in principle. Indeed, weak pressure-induced metallization by band overlap offers a possible reason why a simple Fano line-shape is not entirely appropriate in our case. Physical models aimed to design suitable asymmetric functions should consider that here there are two separate electronic absorption continua of unknown relative magnitudes due to hole-like and electron-like electron-hole pairs, respectively, with which a Raman mode can interfere. On the other hand, all potentially suitable line-shapes are expected to capture the same essential physics, bound to some quantitative evaluation of the asymmetry, here driven by the  $a$  parameter, which in turn originates from the metallic or nearly metallic density of states close to the Fermi level.

In Fig. 3, we report pressure-induced shifts of the two mode frequencies of layered  $\text{SiS}_2$  observed in this work, together with literature experimental values<sup>24</sup> and our freshly calculated DFT values for the layered, octahedral  $P\bar{3}m1$  phase. Comparison between the three different sets of data is very good. As a whole, pressure shift of the frequencies results to be very smooth and slightly sub-linear. Interestingly, our data points for each one of the two modes fit to a single polynomial line, which again confirms that neither phase transitions nor structural changes occur over the entire investigated pressure range, in particular at above 57 GPa. This further confirms that the transformation to a conductive state occurs well within the very same phase, as predicted by DFT investigations.<sup>20</sup>

In Fig. 4 (main panel), we report the integrated Raman intensity of layered, octahedral  $\text{SiS}_2$  per unit acquisition time, as the sum of the two peaks, both Stokes and anti-Stokes, normalized to the integrated intensity of the Stokes diamond peak, as a function of pressure. Data scattering is mainly due to spatial inhomogeneity of the sample. The Raman intensity decreases linearly over the whole 24-57 GPa pressure range leveling off to almost constant above about 57 GPa. As anticipated above, this is most likely evidence of bandgap closing, which increases the optical absorption, and hence scattering volume is decreased and, simultaneously, the Raman cross section itself is decreased upon approaching the conductive state. Because we have no evidence of structural changes from Raman spectra, the clear kink/crossover at about 57 GPa is not of structural origin and must be due to the transition to the metallic or nearly metallic state, which we then locate at about 57 GPa. Above this pressure, the weak yet still well visible Raman peaks are consistent with a poor metal or semimetal, characterized by a low density of states at the Fermi level. The negligible pressure dependence of Raman intensity in the conductive phase signals that density of states at the Fermi level is very weakly pressure dependent, consistent with DFT

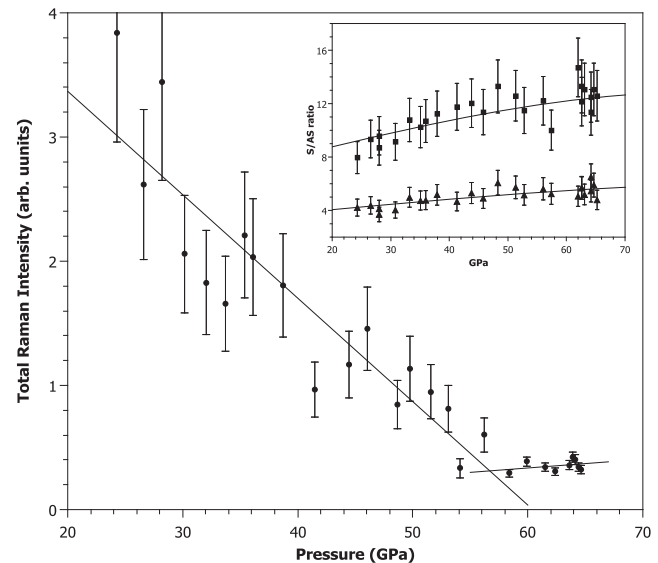


FIG. 4. Main panel: pressure dependence of the total Raman intensity of all the peaks of layered  $\text{SiS}_2$ , both Stokes and anti-Stokes, normalized to the integrated intensity of the Stokes diamond peak. A linear behavior,  $AP+B$ , has been fit to data points at pressures below 57 GPa, with  $A = -8.33 \times 10^{-2} \text{ GPa}^{-1}$  and  $B = 5.03$ . Above 57 GPa, Raman intensity is almost constant. Inset: pressure dependence of the measured Stokes/anti-Stokes intensity ratio for the high (squares) and the low (triangles) frequency Raman peaks, respectively, together with the corresponding theoretical behaviors for non-resonant Raman scattering (continuous lines).

findings.<sup>20</sup> Our results also lead us to model, at least partially, the pressure dependence of the optical absorption coefficient  $\alpha$ . Indeed, in the limit of absorption length being very small with respect to the sample thickness, which is correct at pressures close to metallization,  $\alpha$  increases vs. pressure as  $\alpha = K\sigma/(AP + B)$ . In this relationship,  $P$  is the pressure,  $A$  and  $B$  are the parameters of the linear regression for pressure dependence of the Raman intensity (see Fig. 4),  $K$  is a constant, and  $\sigma$  is the Raman cross section, which also depends on pressure. The linear fit to our data points for Raman intensity at pressures below 57 GPa gives  $A = -8.33 \times 10^{-2} \text{ GPa}^{-1}$  and  $B = 5.03$ .

In the inset of Fig. 4, we also report pressure dependence of the measured Stokes/anti-Stokes intensity ratio for the two Raman peaks (squares and triangles), which fairly agrees with the corresponding theoretical behavior for non-resonant Raman scattering (continuous lines). This ratio increases as a result of pressure hardening of both frequencies. On the other hand, significant mismatch between the experimental and the non-resonant theoretical behavior should be observed when the optical bandgap approaches resonance with the laser line (2.331 eV) upon decreasing it with rising pressure. Our results indicate that such a resonance is still far to be achieved, which in turn totally agrees with DFT simulations showing that the direct bandgap is still very large ( $\sim 4$  eV) when the indirect bandgap closes, at 40 GPa.<sup>20</sup>

In Fig. 5, we finally show the pressure behavior for the effective asymmetry parameter  $M$  of the two Raman peaks together, which we define as  $M = (a_{hf}\sigma_{0hf} + a_{lf}\sigma_{0lf})/m$ , where the parameters  $a$ , line-shape asymmetry,  $\sigma_0$ , and  $m$  are those involved in Eq. (1) and  $hf$  and  $lf$  label the high-frequency and low-frequency peaks, respectively. We found in fact that

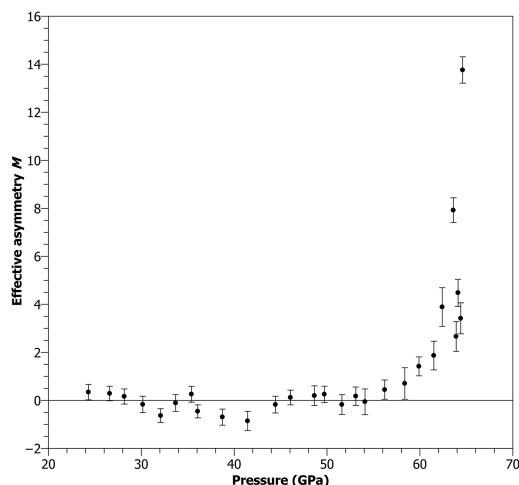


FIG. 5. Pressure dependence of the effective Raman line-shape asymmetry parameter  $M$  (see text).

the effective parameter  $M$  emphasizes pressure-induced asymmetry changes better than the simple asymmetry parameter  $a$  and can be used as a more sensitive probe for the onset of transformation into a possible conductive state. It is then very clear that the effective asymmetry  $M$  is consistent with zero, within error bars, below about 57 GPa, which is what is expected for an ideal semiconductor, and then it suddenly increases to finite values above this pressure, consistent with a metallic or semi-metallic state. Therefore, the pressure behavior of  $M$  points to the transition to a conductive state, whose onset is located at about 57 GPa, which also corresponds to the kink/crossover in the pressure behavior of Raman intensity observed at this pressure.

#### IV. CONCLUSIONS

In conclusion, we discovered a procedure for synthesizing  $\text{SiS}_2$  at high pressures and temperatures. In fact, we have synthesized layered  $\text{SiS}_2$  with Si in octahedral coordination by S, in DACs at 7.5-9 GPa by laser heating and melting together the elements Si and S. Raman spectroscopy has been used for materials' characterization, and experimental results have been compared to new DFT data for the Raman frequencies. The temperature-quenched  $\text{SiS}_2$  compound has been compressed up to about 64 GPa, and Raman spectra have been measured as a function of pressure. Relevant spectral parameters obtained by accurate line-shape fitting of Raman peaks to distorted, asymmetric pseudo-Voigt functions yield remarkable insights into the physics of this important compressed solid. In particular, two effects are of paramount importance here, both strongly indicative of the approaching of a conductive state upon pressure increase: (i) the pressure-induced drop of Raman intensity, with a crossover at about 57 GPa, and (ii) the appearance of asymmetries in the Raman peaks, most likely related to the interference between free or nearly free carriers and optical phonons, suddenly above this pressure. The simultaneous observation of these two effects is suggestive of pressure-induced, continuous bandgap closing in layered  $\text{SiS}_2$  ending up in either a metallic/semi-metallic

state or a narrow bandgap and highly defective semiconductor state, at about 57 GPa, which in turn occurs within the same crystalline phase, with no structural changes. Although optical absorption/reflection and electric transport measurements are certainly required for the definitive assessment and quantitative description of a pressure-induced conductive state in layered  $\text{SiS}_2$  following bandgap closing, our results are overall compatible with recent DFT predictions on electronic/optical properties on this interesting material.<sup>20</sup> This study adds up to the fundamental knowledge of structural and optical properties of dichalcogenides, a class of materials often displaying 2D layered phases at ambient and high pressures. As other layered materials, this one might also offer interesting frictional results under high pressure shear, should that become feasible in the future. In particular, our study adds up to the physics of layered  $\text{SiS}_2$ , which together with other dichalcogenides show an interesting example of the Wilson-like transition, i.e., of a pressure-induced closing of an indirect bandgap followed by metallization. In addition, we open the potential to extend the notion of Raman peak asymmetry due to doping-induced metallicity in semiconductors, already well assessed in the literature,<sup>33,34</sup> to the field of high pressure-induced conductive states in solids.

#### ACKNOWLEDGMENTS

M.S. and F.A.G. performed this research at the Center for Energy Matter in Extreme Environments of the Institute of Solid State Physics of Hefei, Chinese Academy of Sciences, supported by the Chinese Academy of Sciences Visiting Professorship for Senior International Scientists and Recruitment Program of Foreign Experts. M.S. also acknowledges the PRIN project ZAPPING, No. 2015HK93L7, granted by the Italian Ministry of Education, Universities and Research, MIUR, supporting his research in high pressure materials science. Financial support from the National Natural Science Foundation of China (11674330, 11504382 and 11604342) are gratefully acknowledged. A.F.G. was supported by the Chinese Academy of Sciences visiting professorship for senior international scientists (Grant No. 2011T2J20) and Recruitment Program of Foreign Experts. D.P. and R.M. acknowledge the Slovak Research and Development Agency Contract No. APVV-15-0496 and VEGA Project No. 1/0904/15 for supporting their work included in this paper. Part of the calculations was performed in the Computing Centre of the Slovak Academy of Sciences using the supercomputing infrastructure acquired in Project ITMS Nos. 26230120002 and 26210120002 (Slovak infrastructure for high-performance computing) supported by the Research & Development Operational Program funded by the ERDF. Work in Trieste was sponsored under ERC MODPHYSFRICT, Grant Agreement No. 320796.

<sup>1</sup>See [https://en.wikipedia.org/wiki/2D\\_Materials](https://en.wikipedia.org/wiki/2D_Materials) for general information on 2D materials.

<sup>2</sup>N. Bandaru, R. S. Kumar, D. Sneed, O. Tschauner, J. Baker, D. Antonio, S.-N. Luo, T. Hartmann, Y. Zhao, and R. Venkat, *J. Phys. Chem. C* **118**, 3230 (2014).

<sup>3</sup>F. Dybala, M. P. Polak, J. Kopaczek, P. Scharoch, K. Wu, S. Tongay, and R. Kudraw, *Sci. Rep.* **6**, 26663 (2016).

<sup>4</sup>L. Hromadová, R. Martoňák, and E. Tosatti, *Phys. Rev. B* **87**, 144105 (2013).

<sup>5</sup>M. Rifičková, R. Martoňák, and E. Tosatti, *Phys. Rev. B* **90**, 035108 (2014).

- <sup>6</sup>Z. Zhao, H. Zhang, H. Yuan, S. Wang, Y. Lin, Q. Zeng, G. Xu, Z. Liu, G. K. Solanki, K. D. Patel, Y. Cui, H. Y. Hwang, and W. L. Mao, *Nat. Commun.* **6**, 7312 (2015).
- <sup>7</sup>R. Aksoy, Y. Ma, E. Selvi, M. C. Chyu, A. Ertas, and A. White, *J. Phys. Chem. Solids* **67**, 1914 (2006).
- <sup>8</sup>Z.-H. Chi, X.-M. Zhao, H. Zhang, A. F. Goncharov, S. S. Lobanov, T. Kagayama, M. Sakata, and X.-J. Chen, *Phys. Rev. Lett.* **113**, 036802 (2014).
- <sup>9</sup>O. Kohulák and R. Martoňák, *Phys. Rev. B* **95**, 054105 (2017).
- <sup>10</sup>O. Kohulák, R. Martoňák, and E. Tosatti, *Phys. Rev. B* **91**, 144113 (2015).
- <sup>11</sup>J. Evers, P. Mayer, L. Möckl, and G. Oehlinger, *Inorg. Chem.* **54**, 1240 (2015).
- <sup>12</sup>M. S. Silverman and J. R. Soulen, *Inorg. Chem.* **4**, 129 (1965).
- <sup>13</sup>C. T. Prewitt and H. S. Young, *Science* **149**, 535 (1965).
- <sup>14</sup>J. Peters and B. Krebs, *Acta Crystallogr., Sect. B: Struct. Crystallogr. Cryst. Chem.* **B38**, 1270 (1982).
- <sup>15</sup>T. A. Guseva, K. P. Burdina, and K. N. Semenenko, *Khimiya* **32**, 85 (1991).
- <sup>16</sup>M. A. Zwijnenburg, R. G. Bell, and F. Cora, *J. Solid State Chem.* **181**, 2480 (2008).
- <sup>17</sup>D. I. Bletskan, V. V. Vakulchak, and K. E. Glukhov, *Appl. Phys. A* **117**, 1499 (2014).
- <sup>18</sup>Y. Tokuda, T. Uchino, and T. Yoko, *J. Non-Cryst. Solids* **282**, 256 (2001).
- <sup>19</sup>J. Wang, M. Marple, K. Lee, S. Sen, and K. Kovnir, *J. Mater. Chem. A* **4**, 11276 (2016).
- <sup>20</sup>D. Plašienka, R. Martoňák, and E. Tosatti, *Sci. Rep.* **6**, 37694 (2016).
- <sup>21</sup>S. M. Stishov and S. V. Popova, *Geochimija (Russ.)* **10**, 837 (1961).
- <sup>22</sup>M. Lee, J. A. Montoya, and S. Scandolo, *Phys. Rev. B* **79**, 144102 (2009).
- <sup>23</sup>S. S. Naghavi, Y. Crespo, R. Martoňák, and E. Tosatti, *Phys. Rev. B* **91**, 224108 (2015).
- <sup>24</sup>J. Evers, L. Möckl, G. Oehlinger, R. Köppe, H. Schnöckel, O. Barkalov, S. Medvedev, and P. Naumov, *Inorg. Chem.* **56**, 372 (2017).
- <sup>25</sup>H. K. Mao, P. M. Bell, J. V. Shaner, and D. J. Steinberg, *J. Appl. Phys.* **49**, 3276 (1978).
- <sup>26</sup>O. Degtyareva, E. R. Hernández, J. Serrano, M. Somayazulu, H.-k. Mao, E. Gregoryanz, and R. J. Hemley, *J. Chem. Phys.* **126**, 084503 (2007).
- <sup>27</sup>K. S. Andrikopoulos, F. A. Gorelli, M. Santoro, and S. N. Yannopoulos, *High Pressure Res.* **33**, 134 (2013).
- <sup>28</sup>M. Kaczmarzski, O. N. Bedoya-Martínez, and E. R. Hernández, *Phys. Rev. Lett.* **94**, 095701 (2005).
- <sup>29</sup>L. Liu, Y. Kono, C. Kennedy-Benson, W. Yang, Y. Bi, and G. Shen, *Phys. Rev. B* **89**, 174201 (2014).
- <sup>30</sup>Y. Akahama and H. Kawamura, *J. Appl. Phys.* **100**, 043516 (2006).
- <sup>31</sup>P. Giannozzi *et al.*, *J. Phys.: Condens. Matter* **21**, 395502 (2009).
- <sup>32</sup>M. Lazzeri and F. Mauri, *Phys. Rev. Lett.* **90**, 036401 (2003).
- <sup>33</sup>F. Cerdeira, T. A. Fjeldly, and M. Cardona, *Phys. Rev. B* **8**, 4734 (1973).
- <sup>34</sup>D. Olego and M. Cardona, *Phys. Rev. B* **23**, 6592 (1981).
- <sup>35</sup>M. Schmid, H.-P. Steinrück, and J. M. Gottfried, *Surf. Interface Anal.* **46**, 505 (2014).